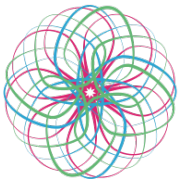

Radboud University

Machine Learning techniques for automatic ocular artifact correction in resting state EEG

Practices and recommendations for the CHDR

Lisa Tostrams (s4386167)
Capita Selecta SOW-BKI209

Research project conducted at the
Centre for Human Drug Research

Supervisors:
dr. J.D.R Farquhar (Radboud University)
dr. Y.M. Miranda (CHDR)
dr.ir. R.J. Doll (CHDR)

Nijmegen, August 2017

Contents

1 Introduction

One of the methods used in the Center for Human Drug Research (CHDR) to asses the effect of a drug is the quantification of resting state electro-encephalography. For the duration of a few minutes, cortical activity is measured in subjects during periods with eyes closed and periods with eyes opened. From the calculated power spectrum of the recorded signals some indications about the state of the central nervous system can be extracted. However, these measurements are often affected by artifacts (e.g. eye and muscle movements). Currently, parts of the EEG recording are rejected when an artifact has been detected (through manual inspection), which means a loss of relevant information.

CHDR is interested in applying Machine Learning techniques to automatically detect and correct artifacts in EEG recordings. The aim of this report is to provide an overview of methods to analyze data from functional brain imaging (EEG) in the presence of (ocular) artifacts, using Machine Learning, filtering and pattern recognition. The purpose of these methods is twofold: to detect the presence of artifacts, and to recover the underlying EEG signal reflecting the true brain electrical activity. Besides providing an overview of methods, this report will recommend performance measurements and a modelling/experimental set up.

First, a short description of usual EEG signals and ocular related artifacts will be given. Then some performance measures will be discussed than can be used to validate methods for artifact correction. In the next section, an overview of correction methods is divided by classes and summarized based on requirements that are relevant to the CHDR. Finally, the discussion will provide a recap and recommend performance measures and methods for the automated correction of ocular artifacts in resting state EEG.

1.1 Electroencephalography

Electroencephalography (EEG) is an electrophysiological method to record electrical activity of the brain. The recording is non-invasive with electrodes placed on the scalp [24], see figure 1 for a typical example of electrode placement. EEG measures voltage fluctuations resulting from ionic current within the neurons of the brain. The joint activity of millions of cortical neurons produce an electrical field that is sufficiently strong to be detected along the scalp. The amplitude of the EEG signal is related to the frequency of activity whether the excitation of the generating neurons is synchronized.

The measured activity reveals oscillatory behaviour in specific frequency bands which are considered to be well-known EEG rhythms [34]. In measuring EEG, the interest typically lies in underlying neural potentials. The various wave forms of the EEG contain clinically valuable information, which make the methods for detection and quantification of characteristics to facilitate interpretation important [25].

1.1.1 Characteristics of EEG

EEG can be described in terms of rhythmic activity and transients. The rhythmic activity is divided into bands by frequency, and activity within a band has been noted to have certain biological significance (see figure 2.a) [34]. The rhythms have for example been noted to reflect different states of vigilance or aspects of cognitive processing.

The amplitude of EEG varies from a few microvolts to approximately 100 μV. The amplitude can be well above this when corrupted by non-cerebral activity. The energy of the EEG signal is more concentrated in the lower range of the spectrum (see figure 3), meaning that 'slower' activity has a higher amplitude. One example is the alpha rhythm, predominantly originating from the occipital lobe during wakeful relaxation with closed eyes. Alpha waves are reduced with open eyes, drowsiness and sleep.

Signals detected by the EEG recording that did not originate from the cortex are considered artifacts. The EEG signal is often contaminated with various physiological factors other than cerebral activity [35]. Ocular movements and eye blinks are some of the most common types of

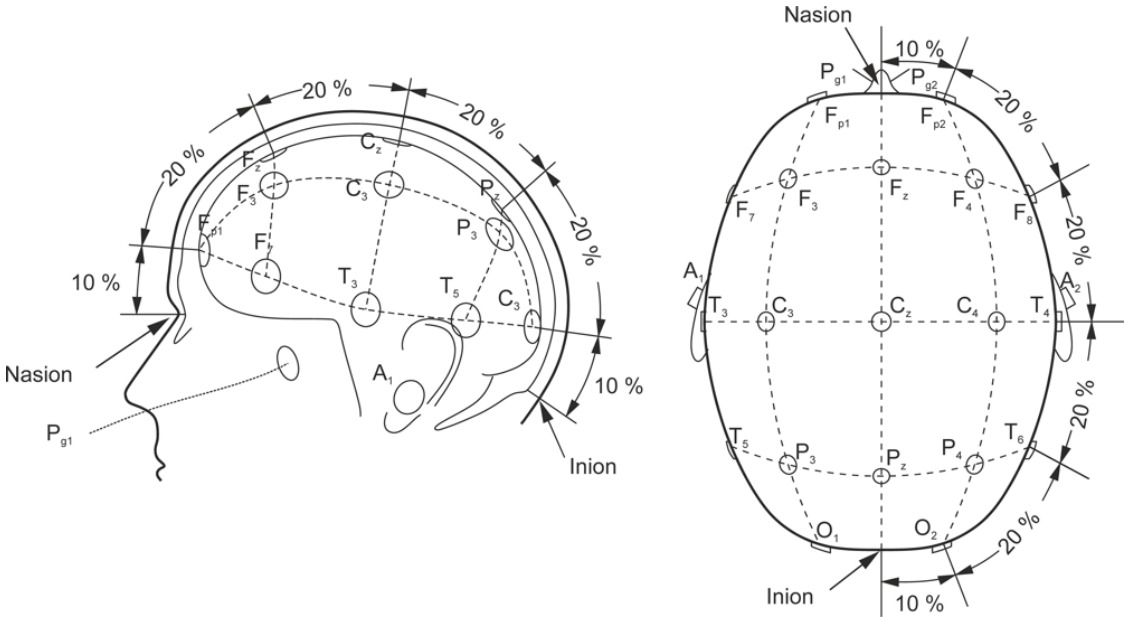

Figure 1: The electrodes for measuring EEG are placed over the scalp based on the International 10-20 system [17]. Using the nasion (located at the top of the nose) and the inion (located at the base of the skull) as reference, the skull is divided into planes. Electrode locations are determined by marking these planes at 10% and 20% intervals. The letters correspond to specific brain regions with, from front to back, Fp, F, C, P and O representing the fronto polar, frontal, central, parietal and occipital areas. The letter T represents the temporal area. A numbering system with odd numbers for the left hemisphere and even numbers for the right hemisphere is uses to differentiate between the sides. The subscript z on the central line stands for zero. Figure obtained from Nicolas-Alonso and Gomez-Gil (2012) [23].

biological artifacts (see figure 2.b). The correction or rejection of artifacts is an important issue in EEG signal processing and a necessary component of most signal analysis. Manual inspection of EEG is a tedious task and automatic scoring is preferred, but often not possible [3].

1.2 Ocular artifacts

The eye forms a electric dipole, where the cornea is positive and the retina is negative. Eye movements change the electrical field around the eye producing an electrical signal known as the electro-oculogram (EOG). EOG signals have mainly a high amplitude and low frequency (see figure 2.b).

The electrical activity produced by eye movement is strong enough to be recorded along with the EEG [9]. Note the relative very high amplitude of the EOG signal as compared to the EEG signals in figure 2. As a result, EEG recordings are often significantly distorted. The eye-movement related voltages propagate to sites along the scalp with an inverse relation to the squared distance from the eyes. About 0.20 of the vertical eye-moment voltage reaches F_z, and this amount decreases posteriorly to about 0.05 at occipital sites.

Blinking is another cause for contamination of the EEG, in a more abrupt manner than eye movement and with a higher amplitude, resulting in sharp pulse artifacts in the EEG signal. When the effect of ocular activity can be estimated, this signal can be removed from the EEG. The resulting corrected signal then reflects more of the true underlying brain activity.

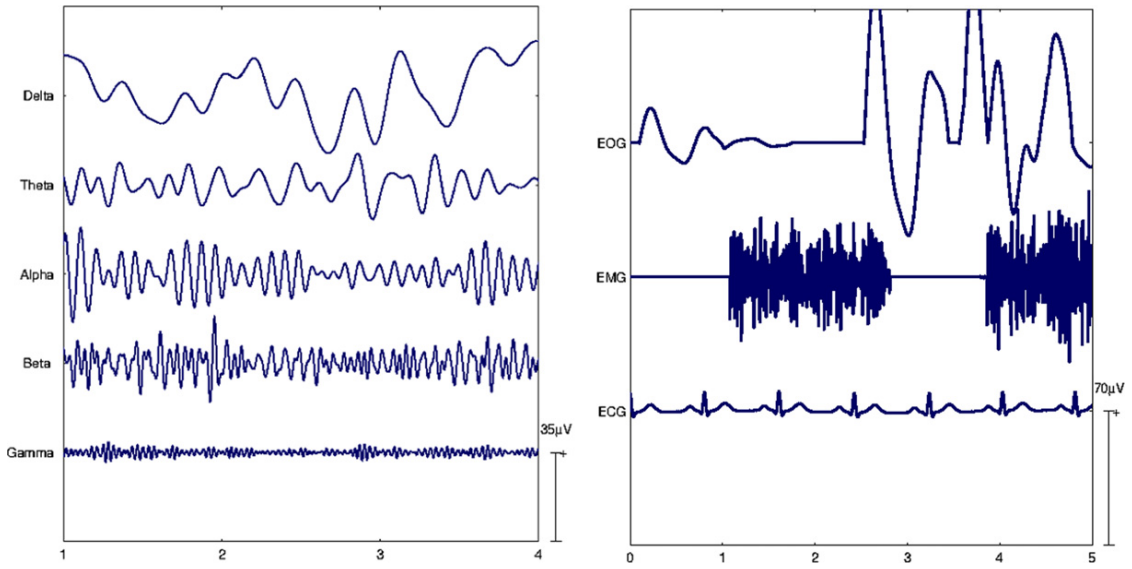

(a) Brain Rhythms *(b) Artifacts*

Figure 2: (a) Examples of five normal brain patterns, from low to high frequencies, with usual amplitude levels. EEG patterns are characterized by their various frequency bands: delta (0.5-4 Hz), theta (4-7 Hz), alpha (8-13 Hz), beta (14-30 Hz) and gamma (30-100 Hz). In very general terms, delta is related to sleep, theta to drowsiness, alpha to relaxed and/or closed eyes, beta to active cognitive processing, and gamma to sensory processing and memory tasks. (b) Examples of three kinds of artifacts: ocular, muscular and cardiac, with usual amplitude levels. Figure from [35].

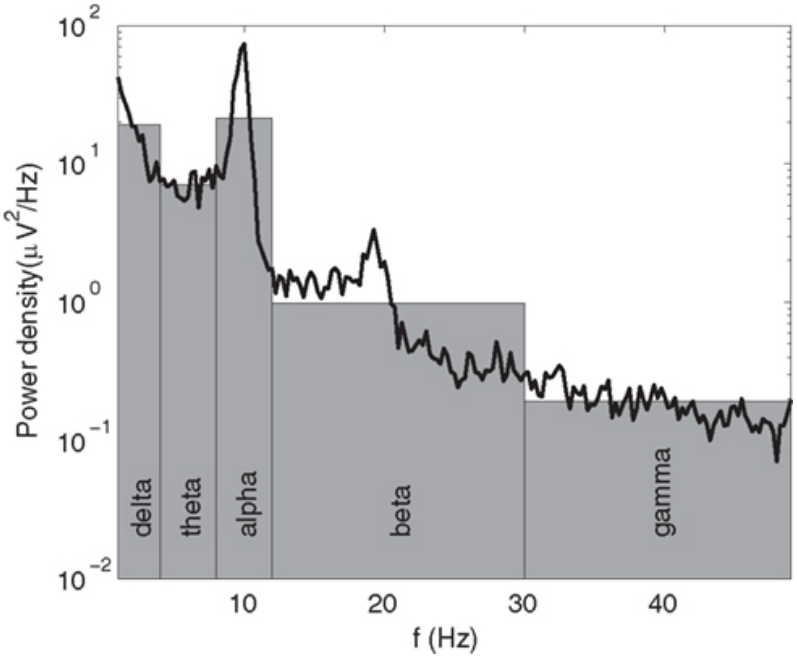

Figure 3: Example of an EEG spectrum (black line) with an approximation of the different EEG pattern band powers, given by the areas of the grey bars. Figure from [36].

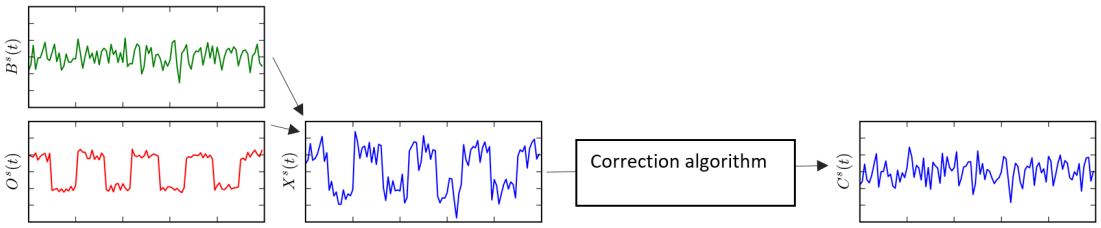

Figure 4: The simulated signal $X^s(t)$ is composed of the simulated 'true' signal $B^s(t)$ and the simulated ocular artifact $O^s(t)$. The corrected signal of the simulated data $C^s(t)$ is obtained by applying an artifact correction algorithm. The improvement of the quality of the data after correction can be computed since the original artifact free signal $B^s(t)$ is known.

2 Performance Evaluation

The greatest challenge for determining the relative efficiency and performance of each artifact correction method is that in 'real' acquired data the uncorrupted desired signal is unknown. The majority of techniques are evaluated with simulated data and thus the validity of conclusions depends on the fidelity of the used model [29]. Methods can first be assessed and compared to other methods by using simulations, but recorded EEG should be used as a final testbed for evaluating the true performance, reliability and reproducibility [35].

2.1 Validation with simulated data

Simulated data can be used for cross-validation of methods, determining optimal values for certain parameters in terms of performance and computation time and as a first guide to validation of corrections. One advantage of using simulated data $X^s(t)$

$$X^s(t) = B^s(t) + O^s(t) \tag{1}$$

where the superscript ^{s} denotes simulated signals and with $B^s(t)$ being the simulated clean signal and $O^s(t)$ being the simulated ocular artifact, as opposed to measured data $X(t)$, is that the quality of the a priori signal and the signal after artifact removal $C^s(t)$ can be assessed through performance measures. For M channels and T measurements, each signal is a MxT matrix.

2.1.1 Percent correlation increase

Correlation is used to describe the degree to which two variables have a linear relationship. The size of the correlation between two timeseries represents how much the two signals behave similarly. A correlation coefficient of near zero between two variables implies that they are linearly independent and a coefficient of near one implies a linear dependence (see figure 5). An increase of the correlation between the correlation of the artifact free signal $B^s(t)$ and the corrected signal $C^s(t)$ compared to the correlation of $B^s(t)$ with the corrupted signal $X^s(t)$ can be used as a measure for improvement.

The Pearson product-moment correlation coefficient ρ of two timeseries $x(t), y(t)$ is defined as

$$\rho = \frac{\frac{1}{T-1}\sum_{t=1}^{T}(x(t)-\mu_x)(y(t)-\mu_y)}{\sigma_x\sigma_y} \tag{2}$$

with σ_x and σ_y being the standard deviations, and μ_x and μ_y the mean values of those timeseries.

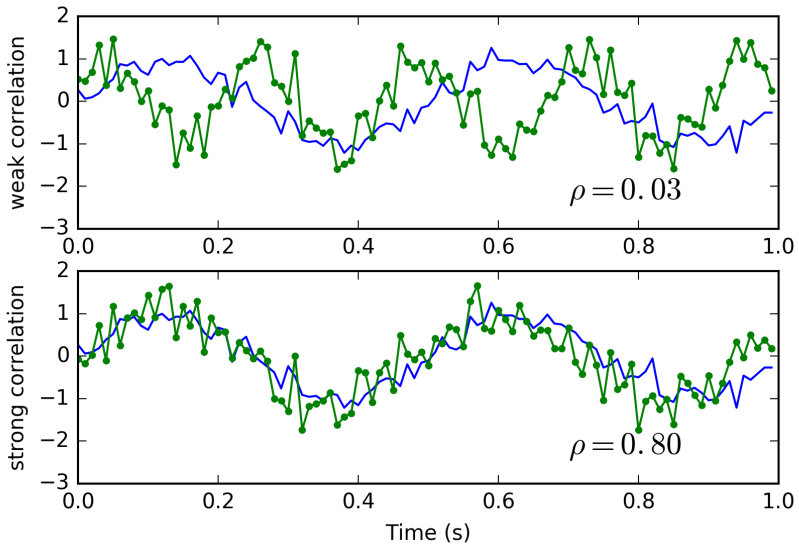

Figure 5: Examples of two signals with a weak correlation (top) and a strong correlation (bottom). The correlation coefficient is 1.0 if there exists a perfect increasing linear relationship, -1.0 in the case of a perfect decreasing linear relationship, and some value in the open interval (-1.0, 1.0) in all other cases, indicating the degree of linear dependence between the variables. As the coefficient approaches zero there is less of a relationship and the variables are closer to being uncorrelated. The closer the coefficient is to either -1.0 or 1.0, the stronger the correlation between the variables.

The percentage increase in correlation after correction is calculated as

$$\frac{\rho_a - \rho_c}{\rho_b - \rho_c} * 100\% \tag{3}$$

where ρ_a is the correlation between $B^s(t)$ and $C^s(t)$ in the parts of the signal where artifacts occur, ρ_c is the correlation between $B^s(t)$ and $X^s(t)$ in the same parts, and ρ_b is the correlation of $B^s(t)$ and $X^s(t)$ in the parts of the signal with known clean data [29].

2.1.2 Signal to noise ratio

The signal to noise ratio (SNR) is a measure of the relative amplitude of the artifact free signal $B^s(t)$ compared to any artifacts (the *noise*) in any recording, see figure 6. The SNR is calculated per channel for both $X^s(t)$ and $C^s(t)$ with regards to the simulated artifact free signal $B^s(t)$ [15]. A higher SNR indicates a better quality signal. For the a priori signal $X^s(t)$, the SNR is defined as

$$SNR_X = \frac{\frac{1}{T}\sum_{t=1}^{T} B^s(t)^2}{\frac{1}{T}\sum_{t=1}^{T}(X^s(t) - B^s(t))^2} = \frac{\sum_{t=1}^{T} B^s(t)^2}{\sum_{t=1}^{T}(O^s(t))^2} \tag{4}$$

Similarly, the SNR of the corrected signal is defined as

$$SNR_C = \frac{\sum_{t=1}^{T} B^s(t)^2}{\sum_{t=1}^{T}(C^s(t) - B^s(t))^2} \tag{5}$$

The gain in SNR after correction can be calculated per electrode as

$$\gamma = \frac{SNR_C}{SNR_X} \tag{6}$$

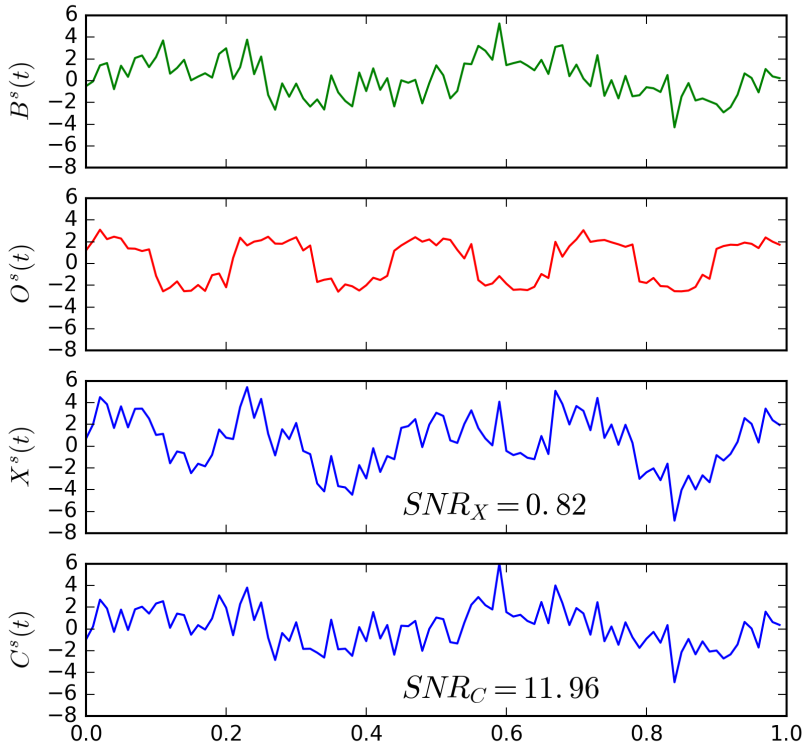

Figure 6: Example of the SNR of some $X^s(t)$ and $C^s(t)$. For $X^s(t)$, the SNR_X is effectively calculated as the relative size of $B^s(t)$ compared to the artifact $O^s(t)$. For the corrected signal, the SNR_C reflects the relative size of $B^s(t)$ compared to any noise left in the signal after correction. In this case, the gain $\gamma = 14.58$ and the overall score $G = 20 * \log_{10}(14.58) = 23.27dB$.

A gain of one depicts no improvement after correction. When the gain is lower than one, the quality of the signal has worsened, and higher than one means the quality has improved. The overall score is obtained by averaging the γ-values of all M electrodes and converting to a Decibel scale

$$G = 20 * \log_{10}\left[\frac{1}{M}\sum_{m=1}^{M}\gamma_m\right] \tag{7}$$

2.1.3 Normalized mean squared error

The normalized mean squared error (NMSE) measures the deviation between the corrected signal $C^s(t)$ and the simulated clean signal $B^s(t)$ [1]. A lower NMSE implies that the corrected signal is more similar to the true artifact free signal. The NMSE is calculated for each channel as

$$NMSE = \left(\frac{\sum_{t=1}^{T}(C^s(t) - B^s(t))^2}{\sum_{t=1}^{T} B^s(t)^2}\right) \tag{8}$$

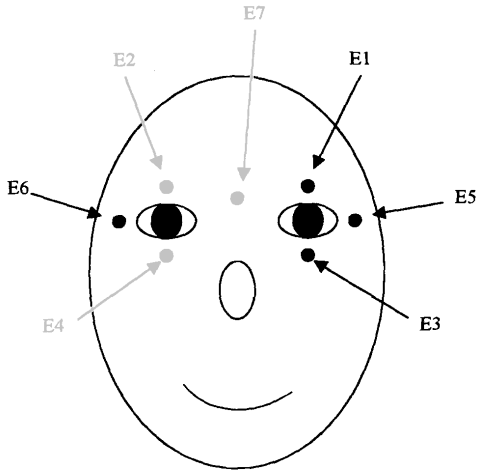

Figure 7: The electrode placement scheme used at the Tilburg symposium [6]. For VEOG the difference between E1 and E3 is computed (E1-E3). For HEOG the difference between E5 and E6 is computed (E5-E6). REOG is computed as (E1+E3)/2.

2.2 Validation with acquired data

In an acquired signal $X(t)$, the true artifact free signal $B(t)$ and the ocular artifact $O(t)$ are unknown. The corrected signal $C(t)$ cannot be compared to $B(t)$ to asses performance. The validation of correction methods on acquired data $X(t)$ depends on a number of factors, of which the most important is the availability of reference channels.

2.2.1 Regression validation (with EOG channels)

The electrooculogram (EOG) is measured from electrodes recording voltage changes close to the eyes, see figure 7. For vertical eye-movements, the vertical EOG (VEOG) is computed as the difference between voltages recorded above and below the eye. Horizontal eye-movements are measured as horizontal EOG (HEOG), the difference between voltages at the left and right outer canthi of the eyes. The radial component (REOG) of the eye-movement is measured by subtracting the average voltage at the eyes from the reference electrodes.

Regression validation is based on the assumption that the EOG and EEG channels are relatively uncorrelated [10]. The correlation between the corrected data and the reference EOG channels is determined by employing least-squares linear regressions where corrected EEG is the criterion variable and the H- and VEOG channels the predictor variables. The resultant absolute unstandardized beta coefficients are tested for relations with repeated measures ANOVA.

2.2.2 Simulate EEG from acquired data (with eye-tracker)

By using eye-tracker data to simulate ocular movements, a signal of ocular movement related artifacts $O^s(t)$ can be simulated in EEG data [15]. These artifacts are superimposed on simulated artifact free EEG signals $B^s(t)$. For subjects, the EEG is recorded at Cz position during a period of no eye movement. This can be verified with simultaneously recorded EOG and eye-tracker data. The resulting average frequency spectrum is used in the model to simulate EEG signals for the specific subject. Eye-tracker data is used to monitor the eye movements and determine the orientation of the source dipole (electrically active tissue).

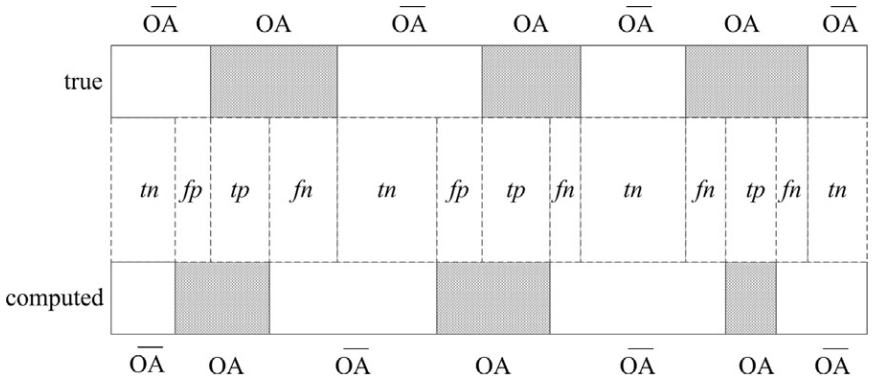

Figure 8: The signal can be manually segmented in regions of Ocular Artifact (OA) zones and non-OA ($\overline{OA}$) zones to establish a ground truth. Comparing the true OA and non-OA zones to the zones computed by thresholding the correction defines the boundaries for the intervals of true positive (tp), true negative (tn), false positive (fp) and false negative (fn). The length of these intervals define the customary tp, tn, fp and fn numbers required for computing sensitivity, specificity and the ROC curve. Figure from [19].

2.2.3 Intentionally corrupted and ground-truth channels (without reference channels)

When there is full control of the EEG recording, two highly correlated signals can be produced: one that is a reference artifact free 'ground-truth' signal, and one signal intentionally corrupted by perturbation of the recording electrode[29]. With these signals it is possible to apply artifact removal methods to the noisy EEG recording and compare the corrected signal to the ground-truth with methods proposed in section 3.1.

2.2.4 Quantitative evaluation of segments with ocular activity (without reference channels)

Correction methods can be turned into classification methods by subtracting the corrected EEG signal from the raw EEG signal and thresholding the result. The resulting binary signal separates segments of the signal (or epoch) into computed zones with ocular artifacts and zones without [19], i.e. computed Ocular Artifact (OA) zones and non-OA zones ($\overline{OA}$) in figure 8.

To quantify classification performance, the ground truth can be defined by manually segmenting signals into true ocular artifact zones and true non-artifact zones, i.e. true OA (OA) zones and non-OA zones ($\overline{OA}$) in figure 8. The boundaries of the true and computed artifact zones define intervals that can be labeled true positive (tp, correctly marked as OA), true negative (tn, correctly marked as non-OA), false positive (fp, incorrectly marked as OA) and false negative (fn, incorrectly marked as non-OA), see figure 8. From the length of these intervals, performance can be quantified by computing sensitivity (the proportion of artifacts that are classified as artifact) and specificity (the proportion of non-artifacts classified as non-artifact), defined as:

$$\text{sensitivity} = tp \text{ rate} = \frac{tp}{tp + fn} \tag{9}$$

$$\text{specificity} = 1 - fp \text{ rate} = 1 - \frac{fp}{tn + fp} \tag{10}$$

Another way to compare the performance of different methods is by plotting the receiver operating characteristics (ROC) curve, a technique for visualizing and selecting classifiers based

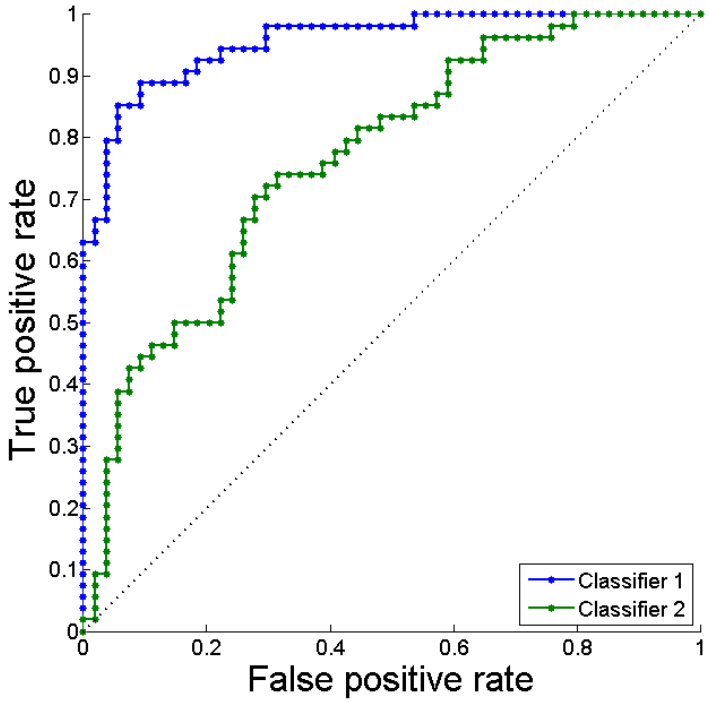

Figure 9: An example of the ROC curve for two classifiers. First, the signals are segmented into zones of true OA and non-OA (see figure 8). The computed OA and non-OA zones can be defined by thresholding the correction applied by some method. For each threshold, a pair of tp and fp rates can be computed. The thresholds range from the boundary that labels the entire signal as a non-OA zone (both tp and fp rates are 0) to the boundary that labels the entire signal as a OA zone (both tp and fp rates are 1). Plotting all pairs of tp and fp rates results in a ROC curve. The dashed line on the diagonal depicts the curve for 'random guessing' classification of zones, and has an Area Under the Curve (AUC) of 0.5. Any method whose curve is above the dashed line performs better than chance, and the more the curve approaches the optimal 1 tp rate vs 0 fp rate (upper left corner, classification results in an AUC closer to 1) the better the performance [11].

on their performance. An ROC curve depics the tradeoff between hit rates and false alarm rates of classifiers when different thresholds for classification are used (tp vs fp rates for different detection thresholds, see figure 9). ROC curves are especially important when considering domains with different classification error costs. This is the case when, for instance, a false alarm (incorrect classification as artifact) is worse than missing an artifact. The results can be visually evaluated per epoch in the artifact affected zones, and quantitatively (area under ROC curve) for several epochs to compare performance between methods.

3 Methods

Methods can be classified in 4 general groups: techniques using regression (EOG correction), filters, component analysis (blind source separation) and source decomposition. In general, each method can be augmented with thresholding for artifact detection, only correcting the signal during the affected intervals to save in computation time and to avoid perturbing the signal in time regions where the signal is not or less corrupted.

3.1 EOG correction [9] [8] [7]

EOG correction generally refers to methods that assume the measured EEG $X(t)$ is a linear combination of the true signal $B(t)$ and ocular artifacts $O(t)$. The proportion of ocular activity present in each channel is calculated by regression. The correction is done by estimating and subtracting the regressed portion of the EOG reference wave forms from each EEG channel resulting in the corrected signal $C(t)$. A coefficient β is calculated as

$$\beta = \frac{\sum_t (X(t) - \mu_X)(EOG(t) - \mu_{EOG})}{\sum_t (X(t) - \mu_X)^2} \tag{11}$$

Where $X(t)$ is the measured EEG and $EOG(t)$ is the measured EOG. The resultant β is then used to correct the EEG measurements by

$$C(t) = X(t) - \beta * EOG(t) - R \tag{12}$$

Where R is the constant from the least-squares formula

$$R = \mu_{EOG} - [\beta * \mu_X] \tag{13}$$

The use of two EOG channels (HEOG and VEOG) in the correction procedure provides a better correction than one, and so multiple regression is often used. EOG correction is known to overcorrect due to bidirectional contamination of the EOG and EEG signals.

Since the EOG is as much contaminated by the EEG as the other way around, a portion of the true EEG is subtracted from the signal as well. Another drawback is the need of propagation factors (i.e. how much of the ocular artifact reaches the electrodes from the front of the scalp to the back) to be constant and the assumption of linearity of the signals. The problems with stationarity of EOG correction can be countered by applying the calculations per epoch. However, this might lead to strange corrected signals if β coefficients strongly differ between subsequent epochs.

3.2 Filtering

Filtering techniques try to adapt the filter in order to minimize the mean squared error between the corrected EEG signal $C(t)$ from the measured EEG $X(t)$, and the desired artifact free signal $B(t)$. The general advantages of filtering is that training data is not needed and that it is automated.

3.2.1 Adaptive filtering [2] [13] [30]

An adaptive filter (AF) is a system with a linear filter that has a transfer function controlled by variable parameters and a means to adjust those parameters according to an optimization algorithm. The adaption of filter parameters is based on minimizing the mean squared error between the filter output $C(t)$ and the desired signal $B(t)$. The AF assumes that the sources of the true signal $B(t)$ and the artifact $O(t)$ are uncorrelated.

The most common adaptation algorithms are Recursive Least Square (RLS) and Least Mean Square (LMS). RLS offers a higher convergence speed but LMS offers computational simplicity. The filter is controlled by a set of coefficients or weights $w(t)$. LMS is based on gradient search according to the equation

$$w(t+1) = w(t) + \mu EOG(t)X(t) \tag{14}$$

where $w(t)$ is the weights vector at sample t, $X(t)$ is the input signal, $EOG(t)$ (the EOG reference channel) is the estimated filters error and μ is the filters convergence factor, or the stepsize. μ controls the rate of adaption and the overall stability of the filter. The weights vector models the contamination of the artifact on the EEG activity, and the estimated artifact is then subtracted from the measured EEG, and the residual is the corrected signal $C(t)$

$$C(t) = X(t) - w^T(t)EOG(t) \tag{15}$$

To remove ocular artifacts with adaptive filtering, separately recorded vertical EOG and horizontal EOG signals are used as reference inputs.

3.2.2 Wiener filtering [18] [12] [30]

Wiener filtering (WF) produces a linear time invariant filter that minimizes the mean square error between the desired signal $B(s)$ and its estimate $C(t)$. The filter parameters are calculated from the spectra of both the signal $\phi_B(\omega)$ and the artifact $\phi_O(\omega)$, which are in turn estimated from the averages of spectra of the measured signals $X(t)$ or by obtaining pure eye blinking components with Independent Component Analysis. Therefore, Wiener filtering does not need a reference signal.

The true signal $B(t)$ and the artifact $O(t)$ are assumed to be stationary linear stochastic processes with known spectral characteristics or known auto- and cross-correlations. The signal and the artifact are assumed to be uncorrelated. The WF produces a probabilistic generative model of the signal and the artifact and a spatial covariance matrix R_k. Based on these parameters, a target event signal is produced and extracted from the observed EEG signal $X(t, f)$ in the time-frequency domain

$$C(t, f) = \hat{R}_{ck}(t, f)\hat{R}_x^{-1}(t, f)X(t, f) \tag{16}$$

$$\hat{R}_{ck}(t, f) = m_k(t, f)\hat{v}(t, f)\hat{R}_k \tag{17}$$

$$\hat{R}_x = \sum_{k=1}^{K} \hat{R}_{ck}(t, f) \tag{18}$$

where f is the frequency of a signal, $m_k(t, f)$ is a posterior probability of the spatial covariance matrix R of the k-th source signal, and $\hat{v}(t, f)$ is an estimation of the variance component of the probability distribution of the source signals. The probabilities are calculated from the power spectral densities of the signal and the artifact, that are in turn estimated from $X(t)$.

3.2.3 Bayesian filtering [31] [35] [30]

Bayesian filtering refers to formulating the problem of estimating the state of a time-varying system that is indirectly observed in terms of Bayesian probability theory. The Bayesian filter produces an estimate $C(t)$ of the value of the true current state $B(t)$ for any t from a probability distribution using all the available information contained in the observation history $X(0), ..., X(t)$. The future states are assumed to be independent of previous states given the current state, and the estimate $C(t)$ for the current state requires formulating a joint probability distribution over all previous measurements. Therefore, Bayesian filtering is limited by its computational complexity.

For every observation $X(t)$ and true state $B(t)$ at any time t the sensor model is defined by $P(X(t)|B(t))$, as depicted in figure 10. These probabilities are usually computed from observed data and therefore a labeled training data set is needed. By applying the Bayes rule

$$P(B(t)|X(0), ..., X(t)) = \frac{P(X(0), ..., X(t)|B(t))P(B(t))}{P(X(0), ..., X(t))}$$

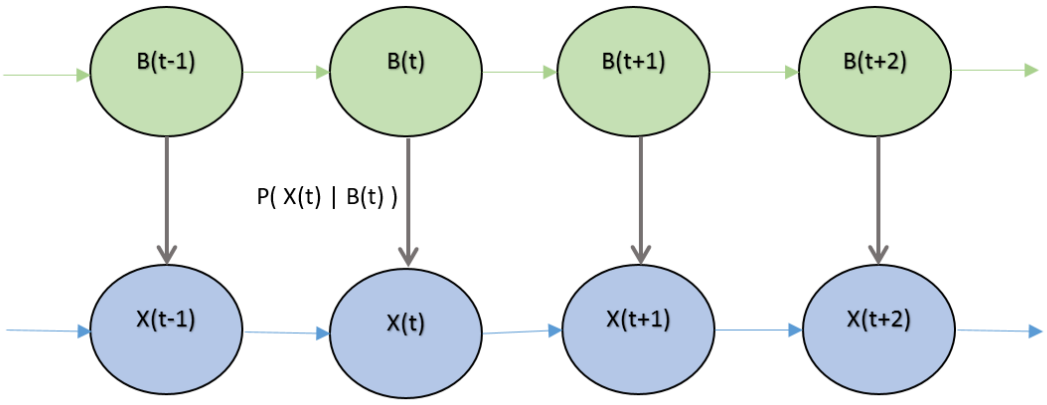

Figure 10: A Hidden Markov Model (HMM), a special case of a Bayesian network that represents sequences of values that are hidden and observations that are related to the hidden values by a (usually stationary) sensor model. The true signal $B(t)$ is unknown, but the observation (the measured EEG) $X(t)$ is related to $B(t)$ by the probability distribution $P(X(t)|B(t))$ defined by the sensor model. Based on the observation history $X(0), ..., X(t)$ the distribution of probabilities for the values of the current true state of the signal $B(t)$ can be computed. The estimate $C(t)$ of the current state is the value for $B(t)$ that is most likely based on the observation history.

the distribution of probabilities for the current state $P(B(t)|X(0), .., X(t))$ based on the observation history is computed. The corrected signal is then

$$C(t) = \arg\max_B P(B(t)|X(0), .., X(t)) \tag{19}$$

This computation step is exponentially complex with the number of observations, and therefore generally impossible to implement. Bayesian filtering assumes the process is Markov, meaning that knowledge of the current state contains all relevant information about the true process. Based on the same notions, the Kalman and particle filters approximate the Bayesian filter.

3.2.4 Kalman filtering [37] [12] [21] [27]

The Kalman filter is a set of equations that provide a means to estimate the state of a process from a series of measurements in a way that minimizes the mean squared error. The algorithm for establishing the true signal $B(t)$ works in a two-step manner: in the prediction step, the filter produces an estimate of the current value and its uncertainty. In the update step, the measurement $X(t)$ is used to update the estimate $C(t)$ using a weighted average between the estimate and the actual measurement (the lower the uncertainty, the higher the weight), see figure 11. The uncertainties about the previous prediction and the measurement are calculated from the measurement and process noise models.

The Kalman filter addresses the general problem of trying to estimate the true state $B(t)$ of a time controlled system from a measurement $X(t)$ at time step t with

$$X(t) = B(t) + \epsilon \tag{20}$$

where the variable ϵ has variance R and represents the measurement noise (in this case, the artifact $O(t)$) at that time. The noise of the time controlled system $B(t)$ is normally distributed with variance Q. Determining the process variance Q is difficult because, in theory, the system that is estimated cannot directly be observed.

The *a priori* state estimate at step t is defined as $C(t-1)$, and the *a posteriori* state estimate is defined as $C(t)$, at time step t given measurement $X(t)$. The goal of the Kalman filter is to compute the *a posteriori* state estimate $C(t)$ as a linear combination of an *a priori* estimate $C(t-1)$ and

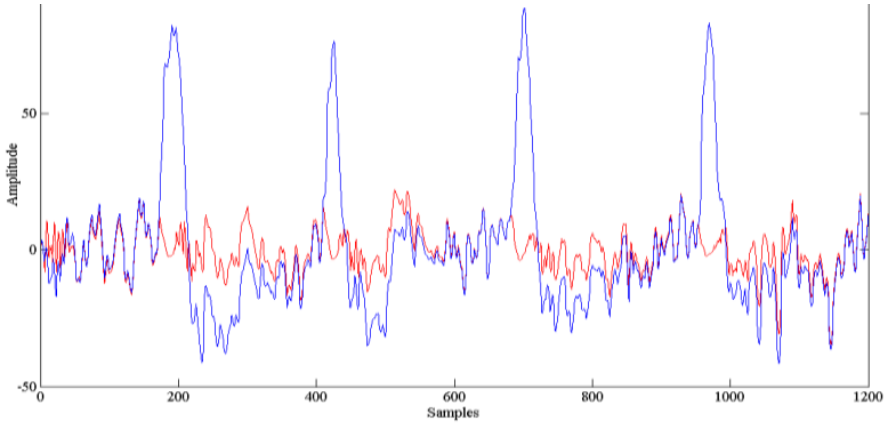

Figure 11: Results from Kalman filter on EEG data [27]. Real EEG (blue) and true EEG estimated by Kalman filter (red).

a weighted difference between an actual measurement $X(t)$ and measurement prediction related to the previous estimate (in this application, simply the previous estimate) $C(t-1)$, given by

$$C(t) = C(t-1) + K_t(X(t) - C(t-1)) \tag{21}$$

K_t is chosen to be the *gain factor* that minimizes the *a posteriori* error estimate P_t

$$P_t = (1 - K_t)P_t^- \tag{22}$$

One form of K_t that minimizes P_t is given by

$$K_t = \frac{P_t^-}{P_t^- + R_t} \tag{23}$$

The difference $(X(t) - C(t-1))$ is called the measurement *residual*. The residual reflects the difference between the predicted measurement and the actual measurement. When the measurement error R approaches zero, the gain K_t weights the residual more heavily. When the estimate error P_t approaches zero, the gain K_t weights the residual less heavily. After each time and measurement update, the process is repeated with the previous *a posteriori* estimates used to project or predict the new *a priori* estimates.

The Kalman filter needs models for measurement noise and process noise variances to produce reliable predictions, but is only dependent on the current measurement and those models, and therefore more efficient in computations than the Bayes filter. If EOG is available, it can be used as an aid in the modeling of the noise.

3.2.5 Particle filtering [30]

Particle filtering uses Monte Carlo sampling to calculate a state transition model of the true signal $B(t)$. N samples are selected from a probability density function, and are weighted according to the amplitude of the probability density function at their sample point. A representative data set is needed to calculate the probability density functions. A large number of samples is needed to properly model the transition probabilities, with the optimal number of samples $N = \infty$ results in a Bayesian filter. The weights of new particles are determined using an update equation that uses the probabilities specified by the sensor model $P(X(t)|B(t))$, and the estimated state $C(t)$ is the mean of the probability density function. Particle filtering depends less on the accuracy of process and sensor models than the Kalman filter, but may converge to the dominance of only a few particles resulting in improper corrections.

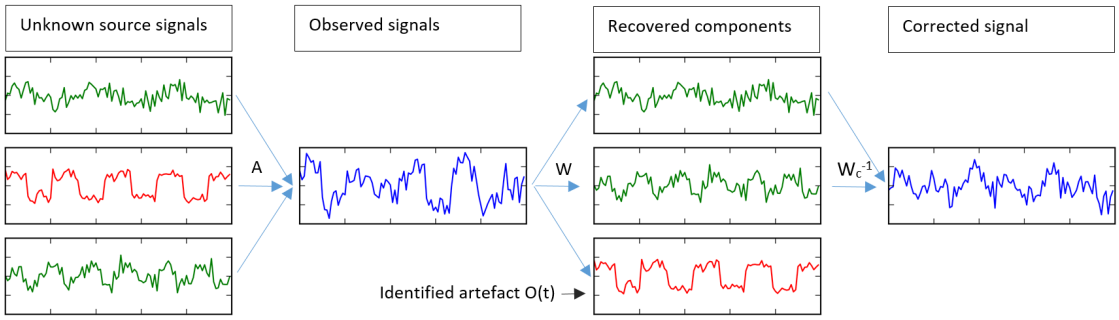

Figure 12: With the (unknown) original sources being true signals in the matrix B (green) and the artifact in O (red), X is a linear combination $X = A[B + O]$ with mixing matrix A. The source signals can be recovered from X with the unmixing matrix W with blind source seperation. When the original sources are known, the artifact O can be selected and the new mixing matrix W_c^{-1} is defined with rows corresponding to the artifact set to zero. The corrected signal matrix C is constructed from the sources using W_c^{-1}.

3.3 Blind source separation

Blind source separation methods are used in signal processing to recover independent sources from signals that record a linear mixture of these sources [22]. BSS uses the observations $X(t)$ to generate an unmixing matrix W that determines an estimation of the original sources, including the artifact. With the original sources being the matrix representations of the true signal B and the artifact O, X is a linear combination $X = A[B + O]$ with mixing matrix A. Given the observation matrix X, the task is to estimate both the mixing matrix A and the original sources $B + O$. Once the mixing matrix A is known, sources can be recovered from X with the unmixing matrix $W = A^{-1}$ with $B + O = WX$. When the original sources of $X(t)$ are found, they can be selected and removed, and the signal is reconstructed without the artifacts to produce $C(t)$ (see figure 12).

BSS techniques generally require more electrodes than expected signal sources, and more time points than the square of the number of electrodes. Either the length of the recording or the sampling frequency can be increased to satisfy this requirement. BSS techniques fall in the class of unsupervised machine learning and do not need training data sets. In principle, the methods are not automatic but can be automated with reference channels.

3.3.1 Principal component analysis [35] [32]

Principal component analysis (PCA) is a statistical method that can be used to capture the variability of data in fewer attributes. PCA uses orthogonal transformation to represent the data in statistical uncorrelated variables called principal components. Reconstructing the data from a number of principal components that is smaller than the number of original variables reduces the variation in the data. PCA tends to identify the strongest patterns in the data.

The variability of an M by T data set X, containing T measurements of M electrodes, can be summarized in an T by T covariance matrix COV, which has entries cov_{pq} defined as:

$$c_{pq} = \frac{1}{M-1} \sum_{m=1}^{M} (X_m(p) - \mu_{X(p)})(X_m(q) - \mu_{X(q)}) \tag{24}$$

where p and q are the p^{th} and q^{th} attribute (column) of the data set X respectively, and represent measurement moments. $\mu_{X(q)}$ and $\mu_{X(p)}$ represent the mean of the columns p and q, and thus depict the average measured EEG over all electrodes at times p and q. The entry cov_{pq} then represents the covariance between two measurement moments.

On the diagonal of the covariance matrix you find the variance in each attribute, or dimension, of the data. The direction of the data with the largest variance is the first Principal Component. The orthogonal direction with the second largest variance is the second Principal Component, and so on. These directions correspond with the eigenvectors W of the covariance matrix COV, ordered by their corresponding eigenvalues $s_1, ..., s_T$. The relative size of the eigenvalues also corresponds to the variance explained by each Principal Component.

The data can be represented in these new dimensions (i.e. rotated) by projecting the data onto the first m eigenvectors W_1 to W_m, resulting in n by m projection Z_m: $Z_m = X[W_1, .., W_m]^{\mathrm{T}}$.The percentage of variance explained p_m by this projection can be computed from the eigenvalues $s_1, .., s_m$:

$$p_m = \frac{\sum_{l=1}^{m} s_l}{\sum_{l=1}^{T} s_l} \times 100\% \tag{25}$$

The data can be reconstructed from this projection to n by T reconstruction $\hat{X}$:

$$\hat{X} = Z_m[W_1, .., W_m] \tag{26}$$

In this reconstruction, p_m percent of variance is captured.

Since patterns caused by likely measurements are probably weaker than patterns caused by unlikely measurements, reduction of dimensionality can eliminate some of the measurement noise. In order to identify the components caused by EOG signals, manual inspection of the components is required. The biggest problem with PCA for EEG applications is that the assumption of orthogonality between neural activity and typical physiological artifacts does not hold.

3.3.2 Independent component analysis [35] [20] [22]

Independent component analysis separates a multivariate signal into additive sub-components using only recorded information, by imposing statistical independence of the signal sources. This independence implies no spatial, temporal or time-frequency correlation between source signals. When applied to multi-channel EEG, the goal of ICA is to unmix signals recorded on the scalp into a linear combination of independent components (IC), each with maximally spatial and temporal independence. The ICA algorithms that exploit higher-order statistics (HOS-ICA) start by applying a orthogonal transformation (PCA) to whiten the data, and then finding the linear transformation that results in the most independent estimated sources. ICA algorithms that apply second-order statistics are based on decorrelating the data in the time domain. Applied to non-averaged multi-channel EEG recordings, ICA has proven very efficient at isolating and removing artifacts. Even when the assumption of independent sources does not exactly hold, ICA has been reported to be successful.

A drawback of ICA is the required intervention of a trained professional to manually identify the components related to artifacts. ICA can be combined with Bayesian classification to be automated, by computing the probability that an epoch represents EEG activity. Again, calculating the necessary probabilities for Bayesian learning is computationally intractable, but they can be estimated by using tree-augmented naive Bayesian networks that construct a maximum spanning tree based on feature dependencies.

When a reference signal is introduced, ICA (then ICA-R) can be automated as well.

3.3.3 Second order blind inference [4] [14] [38]

Second order blind inference (SOBI) uses decorrelation across several time points as its basic computational step. SOBI considers the relationship between components at different time lags and insists that these are decorrelated as much as possible. Similarly to ICA, the data is pre-whitened by PCA and a set of co-variance matrices are calculated at different delays. Using a

joint diagonalizer matrix of the co-variance matrices, the sources can then be estimated. SOBI's ability to resolve correlated activity is essential for ocular artifact detection since artifact signals coming from the two eyes are highly correlated.

The matrix of cross-correlations of the measured (whitened) signal $X(t)$ at time-lag τ is defined as

$$R(\tau) = \mathbb{E}[X(t)X(t-\tau)] = \int_{-\infty}^{\infty} X(t)\overline{X}(t-\tau)\,\mathrm{d}t \tag{27}$$

where $\overline{X}$ represents the complex conjugate. The unmixing matrix W is then computed as the matrix that jointly diagonalizes (rotates) a set of p whitened cross-correlation matrices

$$\{R_W(\tau_i)|i = 1, ..., p\} \tag{28}$$

The diagonalization R_W of a matrix R by matrix W is defined as

$$R_W = WRW^{-1} \tag{29}$$

and is equivalent to the eigen-decomposition of R, where W is the matrix containing the eigenvectors and R_W the diagonal matrix containing the eigenvalues. For a set of matrices, the joint diagonalizer is therefore a form of an average eigenstructure. Computation time for calculating the joint diagonalizer is directly related to the number p of cross-correlation matrices.

The advantage of SOBI is that the time-delay of artifacts propagating over the scalp is considered in the identification of the components. A blink signal reaches the F_p electrodes sooner than, say, the P_z electrode. SOBI is able to identify this relationship over time, if the right time-lags are chosen for computing the cross-correlation matrices. Determining the right lags is related to the expected delay of propagating signals from the front to the back of the scalp. Studies on effects of the chosen delays suggest a set of lags from 1 to 300 ms works best [33] [28]:

$$\begin{aligned}\tau \in \{&1, 2, 3, 4, 5, 6, 7, 8, 9, 10, 12, 14, 16, 18, 20, 25, 30, 35, 40, 45, 50, 55, 60, 65,\\ &70, 75, 80, 85, 90, 95, 100, 120, 140, 160, 180, 200, 220, 240, 260, 280, 300\}\end{aligned}$$

This suggests that the signals needs to be sampled at $1kHz$ or higher.

SOBI can be automated by identifying components that correlate with components from EOG channel recordings. First, the EEG/EOG data is decomposed into a number of components equal to the number of sensors. Second, the sign on all lower and horizontal EOG channels is inverted (i.e. multiplied by -1) and the new data is also decomposed into components. The new components that invert compared to the old are flagged. In this step the components corresponding to EOG signals that do not propagate far from the EOG recording site are identified. Third, the components that correlate above a certain level with the lower and horizontal EOG data and components with high power in the low frequency band are flagged as well. This step identifies the components containing larger eye-movements and blinks that propagate far and are not inverted in the second step. The idea is that the components containing eye activity will correlate more strongly with the lower and horizontal EOG channels than with nonocular components, since these EOG channels reflect primarily ocular motions. The correlation threshold is derived from relations between components originating near the eyes, as identified by geometric relationships contained in mixing matrix W^{-1}. Finally, the flagged components are removed from the data by setting the corresponding rows of the source matrix to zero before multiplying with mixing matrix W^{-1}.

3.3.4 Canonical correlation analysis [35] [30] [5]

Canonical Correlation Analysis (CCA) measures the linear relation between two multidimensional random variables. CCA takes the source vector as the first multidimensional random variable and a temporally delayed version of the source vector as the second multi-dimensional random variable. By looking for uncorrelated components, CCA accounts for temporal correlations. Artifact removal can be introduced by setting the columns of the unmixing matrix that represent artifacts to zero during the reconstruction. CCA does not require independence of the sources.

3.4 Source decomposition methods

Source decomposition methods are applied to single channel recordings. They decompose each individual channel into basic wave forms that represent either the signal or the artifact.

3.4.1 Wavelets [35] [30]

The wavelet transform has been widely uses in the context of EEG denoising. The WT is unable to remove artifacts which overlap in the spectral domain. Good separation of the signal and noise depends on the wavelet basis and its similarity to the source signals, and requires manual selection or comparison to some experimentally-determined threshold. WT can be combined with ICA to overcome shortcomings of both these methods. A drawback is that it is not always true that a source signal can be represented by a single decomposition unit.

3.4.2 Empirical mode decomposition [35] [30] [26]

Empirical Mode Decomposition (EMD) is a technique for non-linear signal processing that aims at decomposing a signal into its basis functions called intrinsic mode functions (IMFs). Signals and artifacts can be represented by one or more IMF. These IMFs can then be used as inputs to an ICA algorithm. The technique is intended for non-linear signal processing, and it is known for its low robustness against noise. Manual selection of artifacts is required.

3.5 Summary

The use of different techniques depends greatly on the availability of reference channels and the assumptions that need to be satisfied. The goal of this report is to research automated methods for artifact correction, and some techniques depend on the presence of EOG channels to operate without manual intervention. See Table 1 for an overview of advantages and disadvantages for each considered method. The used criteria are:

No additional sensors — No additional sensors are needed for this method, e.g. EOG channels or eye trackers. While the addition of sensors is not necessarily a problem at CHDR, a simpler system could be preferred when the experiment has to be set up and broken down multiple times a day, since the sensors need to be placed at the exact same locations each time.

Automated — This method can be automated. Manual selection of artifact affected areas in EEG signals is a tedious task, and generally, an automated method is preferred.

No training data — The implementation of this method does not require training data. Methods that employ supervised machine learning methods require a labelled training data set, with both true signals and artifacts (and their relative occurrence) that resemble the data in the intended application.

No modelling — No a priori modelling of the artifact and or the true signal is needed. In methods that require models of the true signal and the artifact, performance greatly depends on the accuracy of the models and how the models can be generalized to multiple subjects.

Computationally effective — The method has either linear or polynomial time complexity, i.e. execution of the method is computationally feasible.

Table 1: A comparison of the advantages and disadvantages of artifact correction methods.

		No additional sensors	Automated	No training data	No modelling	Computationally effective	No manual checking of result	Easy to implement	Does not assume linearity	Does not assume independence	Insensitive to sign inversion
Regression	EOG correction	✗	✓	✓	✓	✓	✗	✓	✗	✗	?
Filtering	Adaptive filter	✗	✓	✓	✓	✓	✗	?	?	✗	?
	Wiener filter	✓	✓	✓	✗	✓	✓	✓	✗	✗	?
	Bayesian filter	✓	✓	✗	✓	✗	✓	✗	✓	✓	✓
	- Kalman	[1]	✓	✓	✗[1]	✓	✓	✓	✓	✗	✓
	- Particle	✓	✓	✓	✗	✗	✗	✓	✓	✓	?
BSS	PCA	[2]	✗[2]	✓	✓	✓	✗	✓	✗	✗	✓
	ICA	[2]	✗[2]	✓	✓	✓	✓	✓	✗[3]	✗[3]	✓
	ICA+Bayes	✓	✓	✗	✓	✗	✓	✗	✗[3]	✗[3]	✓
	SOBI	✗	✓	✓	✓	✓	✓	✓	✓	✓	✓
	CCA	[2]	✗[2]	✓	✓	✓	✓	✓	✓	✓	✓
SD	WT	✓	✗	✓	✓	✓	✗	?	?	✗	?
	EMD	✓	✗	✓	✓	✓	✗	?	✓	?	?

[1] *does not require models in the presence of EOG reference*

[2] *can be automated in the presence of EOG reference*

[3] *reported to work well even when assumptions are not satisfied*

No manual checking of results	The corrections applied by the method do not need to be checked for over-correction, incorrect convergence of parameters, or perturbation in areas without artifacts.
Easy to implement	Method is easily implementable and runable on all CHDR computers, in Python 3.4 or higher using packages that do not need to be installed separately or can be installed using pyinstaller.
Does not assume linearity	The correction applied by this method does not assume that the measured EEG is a linear combination of the true signal and the artifacts.
Does not assume independence	The method does not assume that the sources of the EEG signal (e.g. EEG signals origination in different brain areas, artifacts) are statistically independent.
Insensitive to sign inversion	Inverting the sign of the artifact signal does not affect the performance of the method. This is the case in, for example, the Kalman filter where correction is based on noise variance, and therefore the filter is unaffected by the sign of the artefact.

4 Discussion

Resting state EEG recordings are used by the CHDR to asses effects of a drug. Since these recordings are often contaminated by ocular artifacts, signal processing is an important part of the analysis procedures. Currently, either the data is accepted as is (including the artifacts), or artifacts are manually selected, and affected parts of the EEG signals are removed completely. Both the need for manual selection and removal of artifacts, and the subsequent loss of possibly relevant information are not preferred. CHDR is interested in applying Machine Learning techniques in general, and a possible first application would be the automated correction of ocular artifacts in EEG. In this report, some methods for performance evaluation are provided to validate the correction of artifacts. Then a number of Machine Learning techniques for the automated detection and correction of ocular artifacts in EEG recordings are discussed. Implementing these methods could mean an improvement in both the ease of the analysis procedure (since it can be automated) and the quality of analysis (since the entire signal can be used after correction). Based on requirements for the analysis of EEG recordings at CHDR, an overview of the advantages and disadvantages of methods is given.

4.1 Recommendations for performance evaluation methods

An important limitation of performance evaluation of correction methods on acquired data is that the true uncorrupted signal is unknown. Consequently, simulated true and corrupted signals provide a manageable means for the in depth testing and evaluation of methods. Performing cross-validation to determine optimal values for certain parameters of the method is most attainable when the corrected signal can be compared to the true signal. To that end, a simulated data set is convenient and beneficial during the development of methods. But reproducibility, as well as performance, should be concluded from applying methods on measured EEG signals [35]. A series of measurements under the same recording conditions should be obtained, producing equivalent EEG and artifact combinations.

4.1.1 Performance evaluation on simulated data

With the use of simulated EEG data, performance of artifact correction methods can relatively easily be compared and the results can be used as a guide for validation. To solve the problem of limited knowledge of the underlying artifact-free brain signal, a semi-simulated EEG data set containing both the pre-contaminated signals and contaminated signals can be used [16]. In this data set, artifact-free EEG signals are manually contaminated with ocular artifacts. Since the data set contains the true recordings, the signal underlying the corrupted data is known, and the performance of different methods can be objectively assessed with the validation methods described in section 2.1. When to use which validation method depends on which aspect of the corrected signal is important. When time-locked patterns are expected to occur and important for analysis, the percent correlation increase (section 2.1.1) determines whether these rhythmic activities have been preserved. The normalized mean squared error (section 2.1.3) also indicates whether patterns have been preserved, but is more affected by whether the amplitude of the signal has changed. The signal to noise ratio (section 2.1.2) validates how much of the artifact has been removed after correction and if the signal has become usable.

Since the signal should not be perturbed in areas without artifacts, the false-hit ratio can be included in evaluation. In the simulated data set, subtracting the true signals from the contaminated signals and thresholding the result, results in a binary time series which indicates where artifacts occur (figure 8). This can be used for plotting an ROC curve (figure 9) and calculating sensitivity and specificity as described on acquired EEG data in section 2.2.4.

4.1.2 Performance evaluation on non-simulated data

Which method to use for validation of correction on acquired data mostly depends on the presence of reference channels that indicate eye-movement and eye-blinks (e.g. EOG channels or eye-

trackers). Both with and without reference channels, a series of EEG data sets recorded under similar experimental conditions is needed to assess the performance and reproducibility of the methods. The performance of artifact correction methods and how to evaluate them greatly depends on the application and the expected SNR of the EEG recordings. Therefore, the validation data should be similar to the data of the intended application.

Since EOG channels are available at CHDR, regression validation is a good option [10]. The magnitude of the relation between the corrected data and the EOG channels is used to measure the proportion of artifacts left in the signal. This method requires manual selection of good and poor corrections of the regression technique.

A validation method that does not require EOG channels is quantitative evaluation of segments with ocular activity before and after correction. An EEG data set labelled by a domain expert is needed, with a binary time series indicating true intervals with and without artifacts. The correction applied by a method is calculated and thresholded to obtain a computed series of intervals with and without artifacts. Performance of the classification of artifacts can be expressed in measures like ROC curve, sensitivity, and specificity.

4.2 Recommendations for ocular artifact correction methods

The different classes of techniques for artifact correction each have their own advantages and disadvantages. EOG correction using regression is a widely used technique, but is limited by assumptions of stationarity and independence of the EEG signals. Filtering on the other hand is more adaptive and easy to automate, but performance heavily depends on the accuracy of the models used by the filters. The advantage of using blind source separation is that no models or training is required, but most BSS methods are harder to automate and make assumptions on the linearity and independence of signals. Source decomposition methods are meant for single electrode recordings, which means that relevant information contained in the relation between electrodes is lost.

The most important requirements for any method to be implemented at CHDR are automation of artifact detection, and correction (as opposed to rejection) of affected signal areas. Additional important criteria as discussed in section 3.5 are related to the simplicity of implementation, such as the need for additional sensors, training data, manual inspection, extensive modelling, required programming libraries and computational complexity. Other criteria are relevant for the expected quality of the corrections, such as assumptions about the signals that need to be satisfied (linearity, independence) and the sensitivity to changes in the artifact. Based on these criteria, an overview is provided in Table 1. Since some requirements are less relevant to the CHDR (such as the need for additional sensors) and others, like automation, are more important, a few methods could be selected. ’

In any time-series analysis, one of the most efficient and simple filters that can be implemented is the Kalman filter. This filter is an approximation of the computationally intractable Bayesian filter. The problem of computing exponentially growing joint probability distributions is solved by making use of process and noise models that specify the likeliness of transitions of the true states and observations given the estimated true states. These models have to be estimated, and the presence of an EOG reference channel can aid in modelling the process and noise signals. The literature on performance of the Kalman filter on EOG artifacts is limited however.

BSS methods provide a more tested and validated class of techniques for the removal of EOG artifacts. ICA, SOBI and CCA can all be automated with the use of reference EOG channels, and have been proven to work well. Of the three, SOBI requires fewest assumptions on independence and non-Gaussian sources and is simplest to automate.

The Kalman filter and SOBI are from the class of unsupervised machine learning techniques and do not require training data. The Kalman filter needs calibration as the choice of expected measurement noise variation matters for the performance, but this can be estimated from reference channels. Compared to many other methods, including SOBI, the Kalman filter is computationally effective and could even be implemented to operate in real-time. The performance of the filter is only as good as the validity of the models, therefore, implementation requires some extensive

modelling and validation of those models.

SOBI is a unsupervised blind method and does not need models to operate. SOBI can easily be automated with the use of EOG reference channels, which are available at the CHDR. This makes SOBI less simple to implement, and performance could depend on correct application of EOG electrodes. In theory, computation time can grow very fast, but this can be improved by choosing the right parameters. The performance is expected to be best when the sampling rate of the EEG signal is at least $1kHz$, and when the number of electrodes is higher than the number of expected sources of signals. Another advantage of SOBI is its ability to recognize time delayed patterns between channels. This makes it a good fit for ocular artifact removal, since ocular signals propagate over the scalp with some small delays. SOBI also makes fewer assumptions regarding the independence of the EEG signals than other blind source separation methods. Either of the methods Kalman filter and SOBI would work for ocular artifact correction, with their performance depending on the expected artifacts that occur in the data, use of EOG reference, and the validity of used models, and the recording set up.

References

[1] L. Albera, A. Kachenoura, P. Comon, A. Karfoul, F. Wendling, L. Sehnadji, and I. Merlet. ICA-based EEG denoising: a comparative analysis of fifteen methods. *Bulletin of the Polish Academy of Sciences - Technical sciences, Polish Academy of Sciences*, 60(3 Special issue on Data Mining in Bioengineering):407–418, 2012.

[2] J.G. Avalos, J.C. Sanchez, and J. Velazquez. *Applications of Adaptive Filtering.* InTech, 2011.

[3] R.W. Becker, J.S. Lukas, M.E. Dobbs, and F. Poza. A technique for automatic real-time scoring of several simultaneous sleep electroencephalogram. *NASA contractor report, National Aeronautics and Space Administration, Washington D.C.*, NASA CR-1840, 1971.

[4] A. Belouchrani, K. Abed-meraim, J. Cardoso, and E. Moulines. A blind source separation technique using second-order statistics. *IEEE Transactions on Signal Processing*, 45(2):434–445, 1997.

[5] M. Borga and H. Knutsson. A canonical correlation approach to blind source separation. *Department of Biomedical Engineering, Linköping University, Linköping, Sweden.*, 2001.

[6] C. H M Brunia, J. Mocks, M. C. Van den Berg-Lenssen, M. Coelho, M. G H Coles, T. Elbert, T. Gasser, G. Gratton, E. C. Ifeachor, B. W. Jervis, W. Lutzenberger, L. Sroka, A. W. Van Blokland-Vogelesang, G. Van Driel, J. C. Woestenburg, P. Berg, W. C. McCallum, P. Dinh Tuan, P. V. Pocock, and W. T. Roth. Correcting ocular artifacts in the eeg: A comparison of several methods. *Journal of Psychophysiology*, 3(1):1–50, 1989.

[7] R.J. Croft and R.J. Barry. EOG correction: a new aligned-artifact average solution. *Electroencephalography Clinical Neurophysiology*, 107(6):395–401, 1998.

[8] R.J. Croft and R.J. Barry. EOG correction: which regression should we use? *Psychophysiology*, 37:123–125, 2000.

[9] R.J. Croft and R.J. Barry. Removal of ocular artifact from EEG: a review. *Journal of Clinical Neurophysiology*, 30(3):5–19, 2000.

[10] R.J. Croft, J.S. Chandler, R.J. Barry, N.R. Cooper, and A.R. Clarke. EOG correction: a comparison of 4 methods. *Psychophysiology*, 42(1):16–24, 2005.

[11] T. Fawcett. ROC Graphs: Notes and Practical Considerations for Researchers. 2004.

[12] J. Ferdous and S. Ali. A comparison of wiener and kalman filters for the artifact suppression from EEG signal. *International Journal of Science and Research*, 6(4):2029–2035, 2017.

[13] P. He, G. Wilson, and C. Russel. Removal of ocular artifact from electro-encephalogram by adaptive filtering. *Medical and Biological Engineering and Computing*, 42(3):407–412, 2004.

[14] C.A. Joyce, I. Gorodnitsky, and M. Kutas. Automatic removal of eye movement and blink artifacts from EEG data using blind component separation. *Psychophysiology*, 41:313–325, 2004.

[15] J. Kierkels, G. van Boxtel, and L. Vogten. A model-based objective evaluation of eye movement correction in EEG recordings. *IEEE transactions on Biomedical Engineering*, 53(2):246–254, 2006.

[16] M.A. Klados and P.D. Bamidis. A semi-simulated EEG/EOG dataset for the comparison of EOG artifact rejection techniques. *Data in brief*, 8:1004–1006, 2016.

[17] G.H. Klem, H.O. Luders, H.H. Jasper, and C. Elger. The ten-twenty electrode system of the international federation. *Recommendations for the Practice of Clinical Neurophysiology: Guidelines of the International Federation of Clinical Physiology*, 2, 1999.

[18] S. Krieger, J. Timmer, S. Lis, and H.M. Olbrich. Some considerations of estimating event-related brain signals. *Journal of Neural Transmission*, 99(1-3):103–129, 1995.

[19] M. Krikove, C. François, and J. Verly. Comparative evaluation of existing and new methods for correcting ocular artifacts in electoencephalographic recordings. *Signal Processing*, 98:102–120, 2014.

[20] P. LeVan, E. Urrestarazy, and J. Gotman. A system for automatic artifact removal in ictal scalp EEG based on independent component analysis and Bayesian classification. *Clinical Neurophysiology*, (117):912–927, 2006.

[21] F. Morbidi, A. Garulli, D. Prattichizzo, C. Rizzo, and S. Rossi. Application of kalman filter to remove TMS-induced artifacts from EEG recordings. *Transactions on control systems technology*, 16(6):1360–1367, 2008.

[22] A. Moreaux and G.D. Iannetti. Across-trial averaging of event-related EEG responses and beyond. *Magnetic Resonance Imaging*, 26:1041–1054, 2008.

[23] L.F. Nicolas-Alonso and J.G. Gomez-Gil. Brain Computer Interfaces, a Review. *Sensors*, 12(2):1211–1279, 2012.

[24] E. Niedermeyer and F.L. da Silva. *Electroencephalography: Basic Principles, Clinical Applications and related fields*. Lippincott Williams & Wilkins, 2004.

[25] P. Nunez and R. Srinisavan. *Electric fields of the brain: the neurophysics of EEG*. Oxford University Press, 2nd edition, 2005.

[26] B. Raghavendra and D. Naraya Dutt. Correction of ocular artifacts in EEG recordings using empirical mode decomposition.

[27] H. Shahabi, S. Moghimi, and H. Zamiri-Jafarian. EEG Eye Blink Artifact Removal by EOG Modeling and Kalman Filter. *5th International Conference on BioMedical Engineering and Informatics (BMEI 2012)*, pages 496–501, 2012.

[28] M.T. Sutherland, J.Y. Liu, and A.C. Tang. Temporal delays in blind identification of primary sometosensory cortex. *Proceedings of the third international conference on Machine Learning and Cybernetics, Shanghai, 26-29 August 2004.*, page 4222, 2004.

[29] K. Sweeney, H. Ayaz, T. Ward, M. Izzetogly, S. McLoone, and B. Onalar. A methodology for validating artifact removal techniques for physiological signals. *IEEE transactions on information technology in biomedicine*, 16(5):918–927, 2012.

[30] K.T. Sweeney, T.E. Ward, and S.F. McLoone. Artifact removal in physiological signals – practices and possibilities. *Transactions on information technology in biomedicine*, 16(3):488–501, 2012.

[31] S. Särkkä. *Bayesian filtering and smoothing*. Cambridge University Press, 2013.

[32] P. Tan, M. Steinbach, and V. Kumar. *Introduction to Data Mining*. Pearson Education Limited, 2013.

[33] A.C. Tang, M.T. Sutherland, and C.J. McKinney. Validation of SOBI components from high-density EEG. *NeuroImage*, 25:539–553, 2004.

[34] W.O. Tatum. Ellen R. Grass Lecture: Extraordinary EEG. *Neurodiagnostic Journal*, 51(1):3–21, 2014.

[35] J.A. Urigüen and B. Garcia-Zapirain. EEG artifact removal – state-of-the-art and guidelines. *Journal of Neural Engineering*, 12(3):23pp, 2015.

[36] S.J van Albada and P.A. Robinson. Relationships between electroencephalographic spectral peaks across frequency bands. *Frontiers in Human Neuroscience*, 2013.

[37] G. Welch and G. Bishop. *An introduction to the Kalman Filter.* Department of Computer Science, University of North Carolina at Chapel Hill, 2006.

[38] L. Zhang, J. Kwok, and B.L. Lu. Applications of second order blind identification to high-density EEG-based brain imaging: a review. *ISNN 2010: Advances in Neural Networks*, 2:368–377, 2010.